Dalton Transactions

ROYAL SOCIETY OF CHEMISTRY

PAPER

View Article Online
View Journal | View Issue

Check for updates

Cite this: *Dalton Trans.*, 2025, **54**, 7851

Luminescence quenching of pyrene-labelled fluorescent dendrons by surface anchoring of ruthenium nanoparticles†

Roberto González-Gómez, [a,b,c] Mireille Vonlanthen, [c] Christian Bijani, [a,b] Catherine Amiens, [a,b] Ernesto Rivera *[c] and Karine Philippot *[a,b]

Received 23rd January 2025,
Accepted 4th April 2025

DOI: 10.1039/d5dt00192g

rsc.li/dalton

Hybrid nanostructures, comprising ruthenium nanoparticles (Ru NPs) and Fréchet-type dendrons of first (G1) and second (G2) generations bearing two and four pyrene units, respectively, and a carboxylic acid group as an anchoring function, have been prepared by taking advantage of the organometallic approach and ligand exchange. Their optical properties have been studied by absorption and fluorescence spectroscopy and compared with those of their counterparts prepared under the same conditions but with pyrene acetic acid and pyrene butyric acid as fluorophores. Pyrene-labelled Fréchet-type dendrons display more pyrene units at a longer distance from the Ru surface than pyrene acetic acid and pyrene butyric acid fluorophores. Interestingly, and unlike pyrene acetic acid- and pyrene butyric acid-derived nanohybrids, the dendron-functionalized Ru NPs exhibit significant to efficient quenching of the pyrene fluorescence (67% for G2 and 94% for G1 with respect to the free dendrons). The quenching effect of the Ru metallic cores on the fluorophore units opens up new prospects for the use of such nanohybrids as antennas for photocatalytic applications.

1. Introduction

As a result of their peculiar properties, the application potential of metal nanoparticles is currently well established.[1] Coupling photoactive entities to metal nanoparticles may present different advantages, such as access to peculiar fluorescence and electron or energy transfer properties that may find applications in various fields such as biosensors,[2] detection,[3] diagnosis and therapy,[4] optoelectronic devices,[5] photonic materials[6] and photocatalysis.[7] As non-exhaustive examples in photocatalysis, the combination of Ru nanoparticles (Ru NPs) with photosensitizers such as the 2-phenyl-4-(1-naphthyl)-quinolinium ion,[8] eosin,[9] or [Ru(bpy)$_2$(4,40-(PO$_3$H$_2$)$_2$(bpy))]Cl$_2$/TiO$_2$ [10] has been reported for the photocatalytic production of hydrogen *via* the water splitting process.

Among the vast family of fluorophores, pyrene is a very powerful fluorescent probe that has been widely used,[11–14] due to its long excited-state lifetime and easy formation of excimers. For instance, pyrene-based conjugated polymers have been found to act as photocatalysts for hydrogen evolution from water.[15] To the best of our knowledge, only a few works have reported on the anchoring of pyrene derivatives bearing appropriate functional groups to the surface of Ru NPs, leading to interesting optical properties. S. Chen and collaborators reported the preparation of Ru NPs functionalized with pyrene moieties by olefin metathesis reactions of carbene-stabilized NPs with 1-vinylpyrene and 1-allylpyrene (Ru = VPy and Ru = APy, respectively).[16] In these constructs, strong intra-particle charge delocalization from the pyrene derivative to the Ru NPs was observed. This extended conjugation platform showed unique optical properties. In the case of Ru = VPy, the obtained construct behaved like a pyrene dimer, whereas in the case of Ru = APy, the fluorescence behaviour was consistent with a monomeric pyrene derivative. These pyrene-functionalized Ru NPs (Ru = VPy and Ru = APy) were employed as chemosensors for the detection of nitroaromatic compounds based on the quenching of their fluorescence.[17–19] J. A. Sullivan and co-workers studied the photophysical properties of Ru NPs functionalized with a fluorescent perylene dye (EP) and silane ligands (ETMS) bound *via* vinylidene linkages. In comparison with the free dye, the Ru NP-bound dye

[a]*CNRS, LCC (Laboratoire de Chimie de Coordination), 205, route de Narbonne, BP 44099, F-31077 Toulouse cedex 4, France. E-mail: karine.philippot@lcc-toulouse.fr*
[b]*Université de Toulouse, UPS, INPT, F-31077 Toulouse cedex 4, France*
[c]*Instituto de Investigaciones en Materiales, Universidad Nacional Autónoma de México, Circuito exterior Ciudad Universitaria, CP 04510 Mexico City, Mexico. E-mail: riverage@unam.mx*

† Electronic supplementary information (ESI) available. See DOI: https://doi.org/10.1039/d5dt00192g

exhibited higher photostability as well as an extended absorption range into the near-UV region, providing enhanced fluorescence in the visible range. Owing to these features, the constructs could find applications in visible-light-driven heterogeneous catalysis in the liquid phase, light-emitting diodes, solar cells, fluorescent biological tags, and as morphologically tuneable materials for metal-to-ligand charge transfer studies in the solid state.[20]

As it has been reported that the physicochemical properties of NPs may benefit from using dendrimers as capping agents,[21,22] and that pyrene group-containing dendrimers and dendrons provide promising materials for luminescence,[23,24] Förster resonance energy transfer and photovoltaic applications,[25–32] we were interested in studying the photophysical properties of Ru NPs decorated by pyrene-labelled dendrons and the quenching efficiencies between the pyrene units and the Ru NPs. Given the absence of the Knight shift with Ru NPs, the coordination of molecules at their surface can be studied by NMR techniques.[33,34] To synthesize the hybrid pyrene-labelled dendron–Ru NPs, we took advantage of the organometallic approach. This synthetic methodology is a powerful strategy to access very small (1–10 nm) metal NPs with controlled and reproducible characteristics that can be used as model systems for studying chemical and physical properties at the nanoscale.[35] Using an olefinic complex as the source of metal atoms, whose ligands are reduced by hydrogen into inert and volatile alkanes (*e.g.* [Ru(COD)(COT)], COD = 1,5-cyclooctadiene, COT = 1,3,5-cyclooctatriene), avoids the presence of by-products that may interact with the NP surface and block the access of the ligand of interest.[36] The latter can be introduced from the start of the synthesis as a stabilizing agent.[37] For instance, rhodamine B-decorated cobalt NPs, synthesised in a one-step procedure, have been a suitable system to study the effect of the metallic core on the optical properties of the fluorophore, and also how the excitation of the fluorophore bound to the surface could induce a modulation of the magnetization of the NPs.[38] However, the ligand of interest can also be introduced in a second step *via* a ligand exchange process.[39] This strategy was used to graft polypyridyl-based Ru (II) complexes *via* phosphonate groups onto the surface of heptanol-stabilized Co_3O_4 NPs[40] and Ru(II) tris(1,10-phenanthroline) complexes onto oleic acid-stabilized core@shell $Fe@Fe_2O_3$ NPs,[41] which provided, in both cases, hybrid nanomaterials that are able to promote photooxidation of water, the bottleneck step in the water-splitting process.

Given the above considerations, we decided to explore the coordination of pyrene-labelled dendrons onto Ru NPs in order to study the resulting fluorescence properties. Herein, we thus report on the functionalization of Ru NPs with Fréchet-type dendrons of the first and second generations, which were specifically designed for this study so that they have two and four pyrene units, respectively, as well as a terminal carboxyl group, which acts as an anchoring function.[42] The study was also conducted on pyrene acetic acid and pyrene butyric acid derivatives as control systems. This series of fluorophores will be referred to as Py–L. Given the ability of Ru NPs to catalyse hydrogenation, in particular of aromatic derivatives,[43] the pyrene-based ligands were not introduced from the start of the synthesis in order to avoid the hydrogenation of the pyrene chromophores, but by ligand exchange on pre-formed Ru NPs. The synthesis of these latter NPs was performed using octanoic acid (OA) as a stabilizing ligand, similar to our previous work on ethanoic acid-stabilized Ru NPs, yet with a longer alkyl chain to facilitate NMR studies. These octanoic acid-stabilized Ru NPs will be noted as OA–Ru NPs hereafter.[44] The dynamic ligand exchange process was monitored *in situ* by DOSY ^{1}H NMR spectroscopy, which allowed us to quantify the number of fluorophores interacting with the OA–Ru NPs. The optical properties of the hybrid systems (denoted as Py–L/OA–Ru NPs) have been studied by absorption and fluorescence spectroscopy under identical *in situ* conditions. As the same ligand-exchange procedure, and the same pre-formed OA–Ru NPs have been used to synthesise the Py–L/OA–Ru NPs hybrid systems, a direct comparison of the optical properties of the latter as a function of the structure of Py–L can be drawn in a reliable manner. To the best of our knowledge, this is the first report on the association of first- and second-generation pyrene-labelled fluorescent dendrons with Ru NPs, which allows the linkage of more photoactive chromophores on the NPs at a longer distance from the metal surface, a key step towards the development of efficient antennas for, *e.g.*, photocatalytic applications.

2. Results and discussion

2.1. Synthesis of the pyrene-labelled dendrons

The pyrene-labelled dendrons of the first and second generations (Py_2–COOH and Py_4–COOH) were synthesized by following a convergent dendrimer synthesis, according to Scheme 1. Standard procedures have been employed to obtain the brominated precursors 1-(4-bromobutyl)pyrene **1** and dendritic benzyl bromide with two pyrene units at the periphery **3**.[27] The methyl ester dendrons of the first- and second-generation **2** and **4**, respectively, were synthesized by the Williamson etherification reaction of the brominated precursors **1** and **3** with methyl 3,5-dihydroxybenzoate. The final acid derivatives, Py_2–COOH and Py_4–COOH, were obtained by hydrolysis of the ester group using potassium hydroxide as a base in a mixture of THF and ethanol as solvent.

2.2. Synthesis and characterization of Py–L/OA–Ru NPs hybrid systems

The hybrid systems of Py–L/OA–Ru NPs were obtained in a two-step procedure, namely by a ligand exchange in solution between pre-formed Ru NPs, synthesized *via* the organometallic approach using octanoic acid (OA) as a stabilizing ligand, and different pyrene-containing molecules, as presented in Fig. 1 (pyrene (Py), and Py–L: pyrene acetic acid (Py–CH_2COOH; Py–Ac), pyrene butyric acid (Py–C_3H_6COOH; Py–But), the first-generation dendron 3,5-bis(4-pyren-1-ylbutyloxy)-

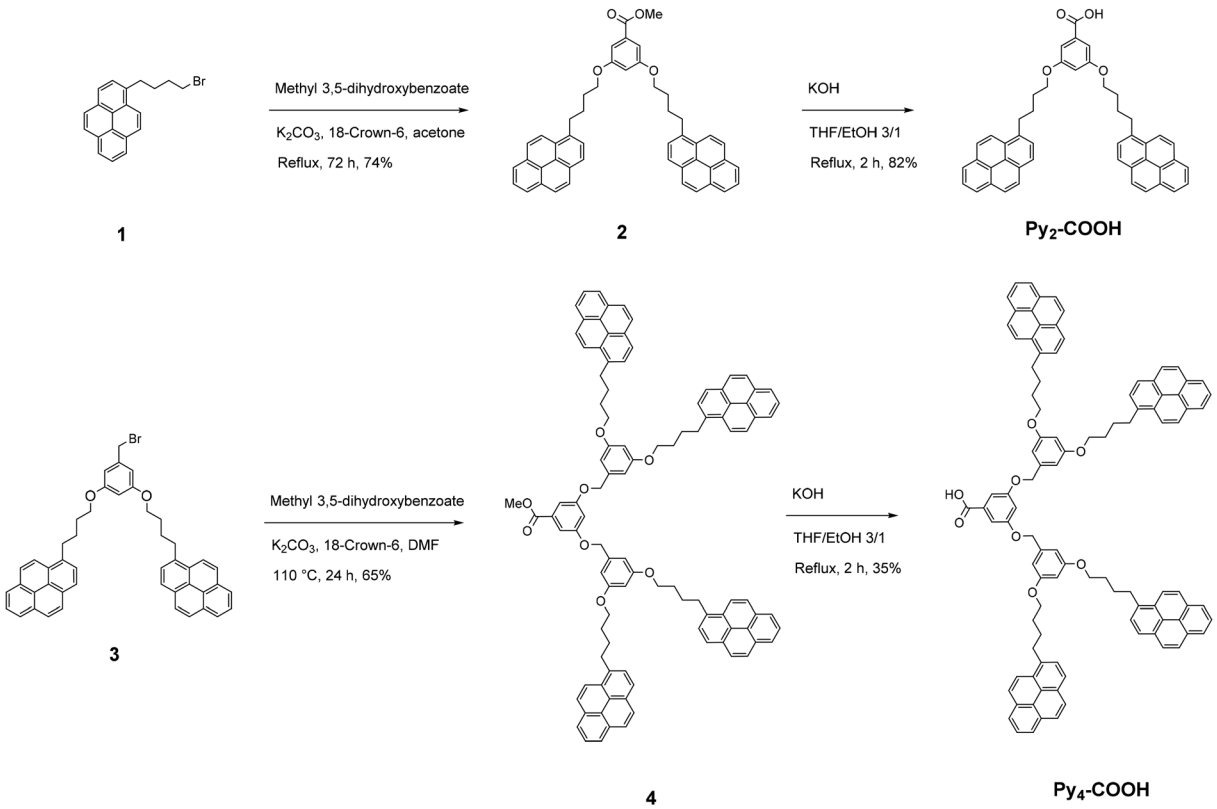

Scheme 1 Synthetic scheme of the pyrene-labelled dendrons Py_2–COOH and Py_4–COOH.

benzoic acid (Py_2–COOH; G_1), and the second-generation dendron 3,5-bis((3,5-bis(4-(pyren-1-yl)butoxy)benzyl)oxy) benzoic acid (Py_4–COOH; G_2)).[26]

The OA–Ru NPs were synthesized by hydrogenation of the olefinic complex [Ru(COD)(COT)] (COD = 1,5-cyclooctadiene, COT = 1,3,5-cyclooctatriene) in the presence of OA as the stabilizing ligand (0.2 molar eq./[Ru]) in pentane (room temperature, 30 min) (Scheme 2, step 1; see synthesis details in ESI section I†).[45] In comparison with free octanoic acid, the ^{1}H NMR spectrum of the OA–Ru NPs displayed only broad peaks in the 2.5–0.5 ppm region, indicating that all the OA interacted with the Ru surface (see ESI Fig. S2†).

Then, the OA–Ru NPs were reacted (under argon; r.t.) with each of the five fluorophores under study (Scheme 2, step 2). For each fluorophore, the influence of the [fluorophore]:[Ru] ratio on the ligand exchange was monitored in solution by DOSY (diffusion-ordered spectroscopy) ^{1}H NMR (see Fig. 2 (*vide infra*) and ESI section II, Fig. S3, S5, and S6, and Tables S1–S4†). This technique allows the resonances of individual components in a mixture to be separated as a function of their hydrodynamic size. On the basis of pulsed field gradient (PFG) NMR, the diffusion rate of a species in a solvent was measured by acquiring a series of spectra at incrementally increasing gradient strengths, resulting in signal attenuation caused by the self-diffusion of the molecules, which is used to calculate a diffusion coefficient (D). As smaller molecules (here, OA free ligands or unreacted Py–L) diffuse more rapidly than larger ones (here, OA–Ru NPs and Py–L/OA–Ru NPs), they display higher diffusion coefficients.

In order to obtain spectra without signals of the free ligands for the sake of clarity, a single ^{1}H NMR spectrum was measured for each Py–L/OA–Ru NPs system by choosing the gradient length, gradient level, and the diffusion delay in a way that the signals of free species would be completely attenuated and those of the coordinated ones still be visible due to slower diffusion. Based on this, the 1D ^{1}H NMR spectra (see Fig. S3† for pyrene and Fig. S4† for pyrene–acetic acid (Py–Ac) as a typical example of Py–L) display only the signals from the coordinated molecules. As the same ligand-exchange protocol and the same pre-formed OA–Ru NPs were used to introduce all tested fluorophores, the comparison between the hybrid systems formed is reliable.

As Py does not have any carboxylic acid groups to promote its anchoring at the NP surface, it was used as a control to check for any π-interactions that might occur between aromatic rings and the NPs. A sweep of the [Py]:[Ru] ratio from 0.05 to 0.2 in benzene-d_6 did not show any interaction of Py at the NP surface (see ESI, Fig. S3†). Indeed, in 1D DOSY ^{1}H NMR spectra, no peak can be observed in the aromatic region, whatever the number of Py equivalents added. The only peaks observed are located in the 2.5–0.5 ppm region and are attributed to coordinated OA, as for the native NPs (see ESI Fig. S2†). The absence of the ligand exchange between surface-bound OA and Py thereby discards the potential anchoring of this fluorophore at the NP surface *via* π-interactions.

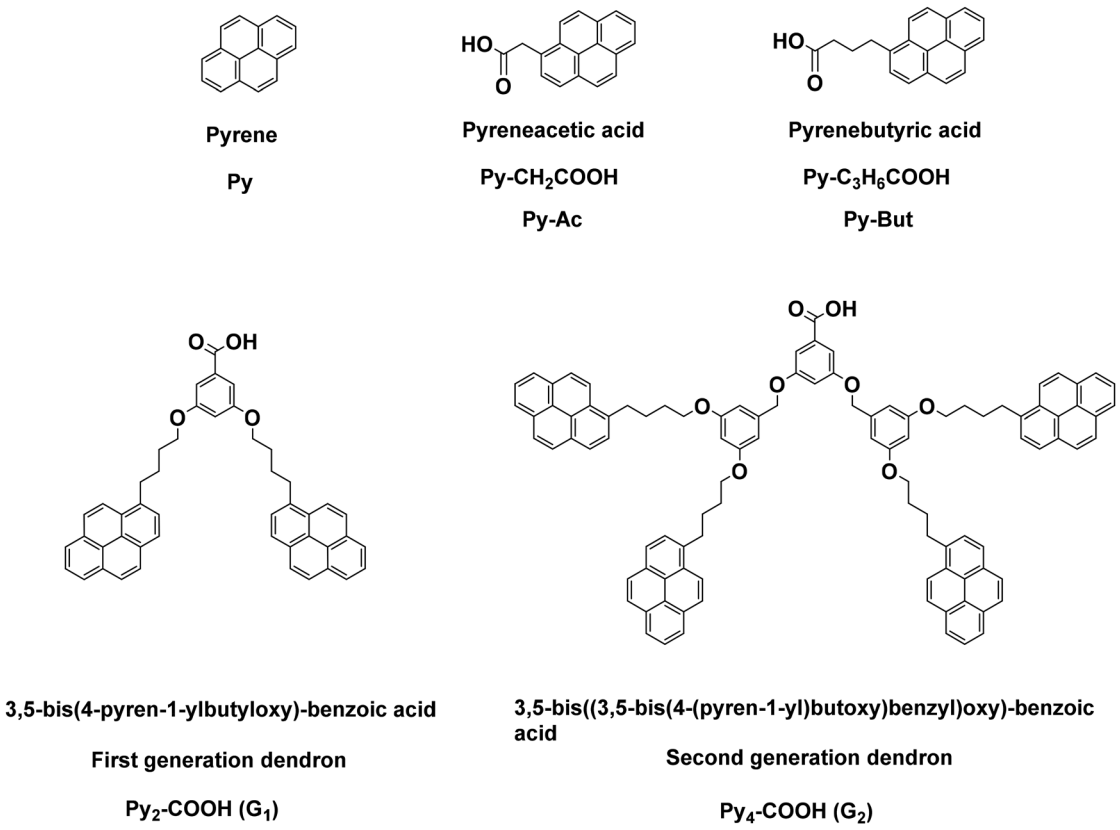

Fig. 1 Pyrene and Py–L fluorophores used in this study.

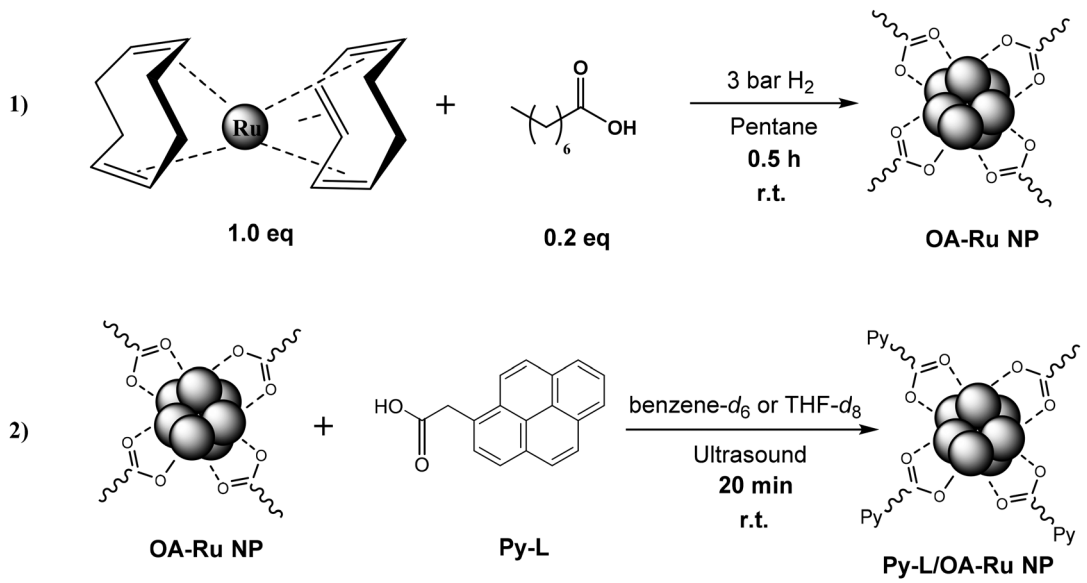

Scheme 2 (1) Synthesis of the OA–Ru NPs; (2) synthesis of the Py–L/OA–Ru NPs hybrid systems by ligand exchange exemplified with Py–Ac. Not all ligands are drawn on the NP surface, as their ratio depends on the Py–L used.

The ^{1}H NMR (THF-d_8) spectrum monitoring of the addition of Py–Ac or Py–But ligands to a colloidal suspension of OA–Ru NPs, with a sweep of the [Py–L] : [Ru] ratio in the range from 0.05 to 0.2, revealed that this time a ligand exchange occurred. Broad peaks were observed in the 8.4–7.9 ppm range, the intensity of which increased with the [Py–L] : [Ru] ratio, and this can be attributed to the pyrene group of the fluorophore in interaction with the NP (see ESI Fig. S4† for Py–Ac as a typical example). In

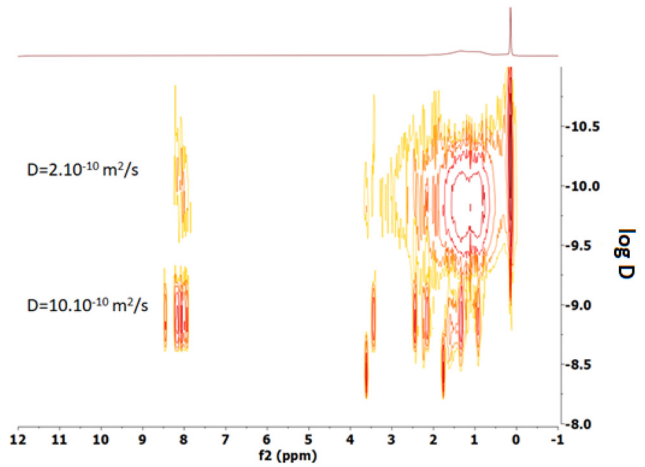

Fig. 2 2D DOSY ^{1}H NMR spectrum (THF-d_8) of the reaction between OA–Ru NPs and 0.05 eq. of pyrene butyric acid (Py–But; Py$(CH_2)_3$COOH); D = 10 × 10^{-10} m^2 s^{-1} = diffusion coefficient of free Py–But; D = 2 × 10^{-10} m^2 s^{-1} = diffusion coefficient of Py–But interacting with Ru NPs.

parallel, the intensity of the peaks of OA (in the 2.5–0.5 ppm region) decreased with the increase of the [Py–L] : [Ru] ratio, indicating the progressive release of OA in solution and thus attesting to the ligand exchange. DOSY ^{1}H NMR spectra (see Fig. 2 and S5† for Py–But and Py–Ac, respectively) confirmed the interaction of the fluorophore with the NP surface, with diffusion coefficients nearly five times lower for the interacting species (*ca.* 10 × 10^{-10} m^2 s^{-1} and *ca.* 2 × 10^{-10} m^2 s^{-1} for the free Py–L and interacting species, respectively). The integration of the different peaks allowed quantification of the ligands interacting with the NPs (see ESI Tables S2 and S3† for Py–Ac and Py–But, respectively). The addition of 0.2 eq. of the fluorophore led to exchange ratios (ligand out (OA)/ligand in (Py–L)) above 1 in each case, with a larger value determined for Py–But (*ca.* 2.3) than for Py–Ac (*ca.* 1.8). This can be explained by the steric hindrance of the fluorophores in comparison with OA.

A similar study was performed to follow the reaction between the first-generation dendron (Py_2–COOH; G_1) and OA–Ru NPs. In terms of steric hindrance, Py_2–COOH can be compared to Py–Ac, as it also has a rigid carboxylic acid anchoring group. However, Py_2–COOH presents the interest of having two photoactive units *vs.* one in the two previous fluorophores. A sweep of the [Py–L] : [Ru] ratio was carried out from 0.05 to 0.15. The coordination of the fluorophore and release of OA could be observed and quantified by DOSY ^{1}H NMR spectroscopy (see ESI, Fig. S6 and Table S4†). Despite a lower quantity of fluorophore added (0.15 eq. *vs.* 0.2 eq. for the two previous cases), the number of Py–L interacting with the NPs (0.069 eq.; see ESI Table S4†) is already higher than in the case of Py–Ac and Py–But (0.062 eq. for Py–Ac and 0.042 eq. for Py–But as shown in ESI Tables S2 and S3,† respectively). However, the quantity of OA released per fluorophore is much lower in this case (0.55 *vs.* 1.7 for Py–Ac and 2.3 for Py–But; see Tables S4, S2 and S3,† respectively), suggesting that Py_2–COOH interacts mainly in outer coordination shells. Concerning the second-generation dendron (Py_4–COOH; G_2), a saturation phenomenon was observed in the ^{1}H NMR spectra in the relevant concentration range, which can be explained by the high molecular weight of Py–L. Therefore, it was not possible to obtain relevant proof of its interaction with the NPs by ^{1}H NMR spectroscopy. However, as will be discussed later, the addition of this dendron to a solution of OA–Ru NPs led to a drastic modification of its optical properties. This phenomenon cannot be explained without any close interaction between the two entities.

To sum up, the NMR studies described above evidenced that unsubstituted pyrene does not displace the OA ligand interacting with the NP surface. In the following, we will consider that this fluorophore does not interact with the NP surface and thus can be used as a control for the fluorescence study. The incorporation of a carboxylic acid group into the Py fluorophore (Py–L) is a driving force for ligand exchange, thus providing hybrid Py–L/OA–Ru NPs systems. This ligand exchange was observed to depend on the fluorophore structure and flexibility. The results show that a higher proportion of Py–Ac (*ca.* 31%) than Py–But (*ca.* 21%) interacts with the NP surface, in agreement with their relative steric hindrance. Interestingly, a higher proportion of G1 (*ca.* 50%) interacts with the NPs, which suggests that once a certain steric hindrance limit is reached, second-shell interactions set in. This phenomenon might be favoured by the molecular structure of G1 and can be expected to occur for G2 as well, due to the increased mobility imparted to the Py unit by the butyl chains, as they are further apart from the coordinating carboxylic acid function in comparison to Py–Ac and Py–But.

2.3. Fluorescence studies of the Py–L/OA–Ru NPs hybrid systems

The study of the optical properties of the free Py–L and Py was performed in dry THF solutions under an inert atmosphere. The absorption spectra of the studied compounds are shown in the ESI (Fig. S7–S11†). The absorption bands of the pyrene moiety of the free Py–L were observed at 277 and 344 nm, and those of the free Py at 274 and 336 nm, corresponding to the $S_0 \rightarrow S_3$ and $S_0 \rightarrow S_2$ transitions, respectively. The extinction coefficients of the absorption band at 344 nm were determined to be 39 000 and 46 000 M^{-1} cm^{-1} for Py–Ac and Py–But, respectively. For the dendronized pyrene derivatives, the extinction coefficient values of 87 000 and 170 000 M^{-1} cm^{-1} were obtained for the first-generation Py_2–COOH (G_1) and second-generation Py_4–COOH (G_2) dendrimers, respectively. With all these fluorophores, the mean extinction coefficient value for one pyrene unit is thus about 43 000 M^{-1} cm^{-1}, which corresponds well to the previously reported values for pyrene derivatives.[25]

The fluorescence emission spectra of the Py–L were studied under the same conditions as above (dry THF solvent and inert atmosphere) with an excitation wavelength of 344 nm. In the fluorescence spectra of Py, Py–Ac and Py–But, only the monomer emission band was observed at 378 nm, since those compounds are composed of only one pyrene unit and diluted solutions were used (Fig. S12–S14†), similarly to the free Py (λ_{em} = 374 nm and λ_{ex} = 336 nm). In the case of G_1 and G_2, pyrene monomer (M) emission as well as a broad excimer (E)

emission were observed at λ_{em} = 378 and 480 nm, respectively, due to a higher local pyrene concentration (Fig. 3, S15 and S16†). The ratio of the excimer emission intensity (I_E) *vs.* monomer emission intensity (I_M) increased for the second-generation dendrimer, as previously reported for similar compounds.[25]

The optical properties of the hybrid systems (Py–L/OA–Ru NPs) have been studied by absorption and fluorescence spectroscopy. As the same pre-formed OA–Ru NPs were used in each case, a direct comparison of the optical properties of the hybrid nanostructures could be carried out. Different types of quenching phenomena are expected to occur depending on the molecular structure of the fluorophores.[46,47] In the case of Py, only a collisional quenching effect is expected, as the NMR study could not evidence any interaction with the NPs. For the Py–L fluorophores that contain a carboxylic acid group, a direct effect of the Ru NPs on the fluorescence properties of the fluorophores by both fluorescence energy transfer and electron transfer can be expected, as a ligand exchange occurs at the surface of the NPs, leading to the anchoring of the fluorophores.

Preliminary experiments were carried out using OA–Ru NPs and Py. The emission spectra recorded for different [OA–Ru NPs] : [Py] ratios (λ_{exc} = 336 nm), increasing the amount of Py from 0.05 to 0.3 eq., showed that the NPs were acting as a quencher of the emission of Py. The kinetics of the collisional quenching was studied. The Stern–Volmer constant (k_{SV}) for the quenching of Py fluorescence by OA–Ru NPs was calculated using eqn (1):

$$\frac{I_0}{I} = 1 + k_{SV}[\text{OA} - \text{Ru NPs}] \quad (1)$$

where I_0 is the fluorescence emission at λ_{em} = 374 nm in the absence of the NPs, I is the fluorescence emission (λ_{em} = 374 nm) of the solutions containing Py and NPs, k_{SV} is the Stern–Volmer constant and [OA–Ru NPs] is the concentration of the quencher (here, OA–Ru NPs). The variation of I_0/I as a function of [OA–Ru NPs] showed linear behaviour (see ESI Fig. S12†), and the Stern–Volmer quenching constant k_{SV} could be determined from a linear fit of the experimental data: $k_{SV} = 6.15 \times 10^5\ M^{-1}$.

For all other Py–L fluorophores, the carboxylic acid function led to an efficient interaction of the fluorophores with the NPs, as demonstrated by the NMR experiments. However, some free Py–L is still present in the mixture due to equilibrium conditions. The photophysical studies were performed with different [OA–Ru NP] : [pyrene unit] ratios, at λ_{exc} = 344 nm. In all cases, a quenching of the pyrene chromophore emission was observed. The quenching efficiency (Q) resulting from the formation of the Py–L/OA–Ru NPs hybrid was quantified by comparing the fluorescence emission of the fluorophore at λ_{em} = 378 nm with (I) and without the quencher (I_0), using eqn (2):

$$Q = \left(1 - \frac{I}{I_0}\right) = \left(1 - \frac{I}{(m_{\text{Py–L}})([\text{Py} - \text{L}]) + b_{\text{Py–L}}}\right) \quad (2)$$

The I_0 value was determined using a calibration curve (emission intensity at λ_{em} = 378 nm *vs.* concentration) of the corresponding Py–L (see ESI Fig. S13–S16†), where [Py–L] is the concentration of the pyrene ligand, $m_{\text{Py–L}}$ is the slope, and $b_{\text{Py–L}}$ is the intercept of the calibration curve in the excimer emission range. When the concentration of Py–L was increased, a higher concentration of the free ligand remained in the solution, leading to an apparent decrease in the quenching efficiency (Tables S5 and S6†). Therefore, the discussion will focus on the experiments made with the lowest quantities of the introduced fluorophore, namely [OA–Ru NPs] : [Py–L] = 0.116.

In the case of Py–Ac, which could be considered a dendron of zero generation, a significant (78%) quenching of its emission was observed (see ESI, Fig. S17, Table S5†), which con-

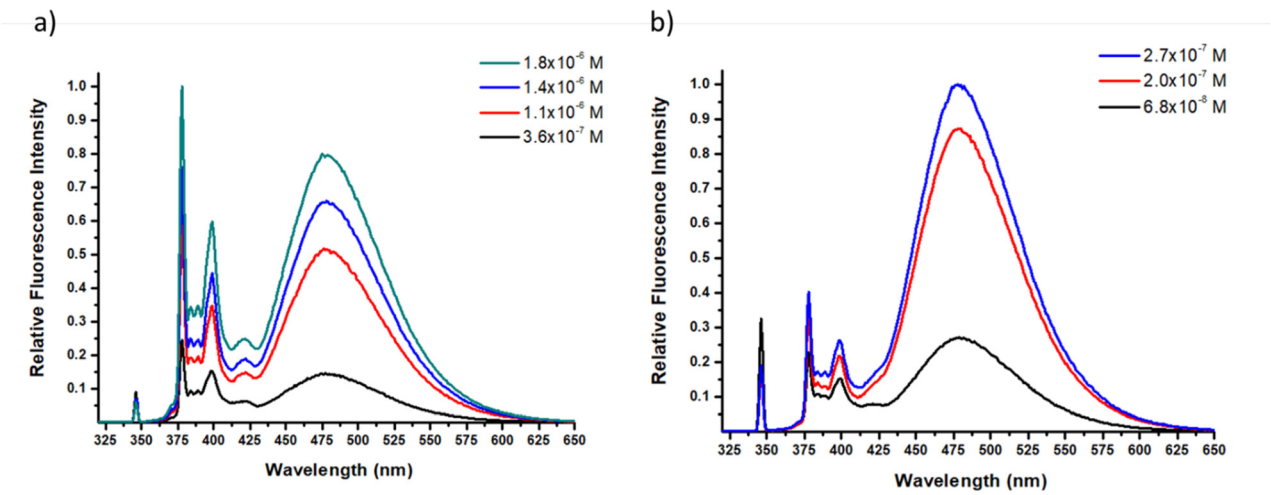

Fig. 3 Emission spectra of (a) Py_2–COOH (G_1) and (b) Py_4–COOH (G_2) measured in THF solutions under argon at different concentrations (λ_{exc} = 344 nm).

firmed that efficient energy or electron transfer occurs when the fluorophores interact with the NPs.

Significant quenching was also observed when the OA–Ru NPs were functionalized with Py–But. However, the NMR studies revealed that the incorporation of this ligand was less efficient than the incorporation of Py–Ac (Tables S2 and S3†). The alkyl chain length also has a significant effect, as the NP quenching efficiency generally decreases as the distance between the fluorophore and NPs increases, which was expected here when comparing Py–Ac and Py–But. Accordingly, a fluorescence quenching of only 69% was observed under the same measurement conditions, namely for an [OA–Ru NP] : [Py–But] ratio of 0.116 (see ESI, Fig. S18, Table S6†).

Then, two Fréchet-type dendrons of first and second generations bearing a carboxylic acid group (Fig. 1, Py_2–COOH and Py_4–COOH) were reacted with pre-formed OA–Ru NPs. The obtained emission spectra are shown in Fig. 4. It was observed that the monomer and the excimer emission of Py_2–COOH were both drastically quenched by the NPs. Using eqn (2), a quenching efficiency of 94% was calculated for 0.05 eq. of added dendron per Ru content (*i.e.* [OA–Ru NP] : [pyrene unit] of *ca.* 0.06). This result is particularly interesting as the NMR study suggested that G1 pyrene units interacted mainly in a second coordination sphere around the NPs and hence should be more distant from the metal surface than Py–Ac and Py–But. This may be explained by the larger proportion of G_1 actually interacting with the NPs as a result of its specific structure, as discussed above.

The second-generation dendron, Py_4–COOH, with four fluorescent pyrene units in the periphery, and one carboxylic acid anchoring group, has a larger molecular structure. Due to the complexity of this system, it was not possible to follow the ligand exchange by ^{1}H NMR experiments. Solutions were prepared to obtain a fluorophore concentration that could be used in the calibration curve, which was previously plotted (2.2×10^{-7} M) (Fig. 5). Upon excitation at 344 nm, the NP quenching performance was quantified by comparing the fluorescence emission of the dendron at 378 nm in the presence (I) and in the absence (I_0) of the quencher, using eqn (2). A maximum quenching of 67% was observed in this case (Fig. 5 and Table 2).

When comparing the effect of the NPs on G1 and G2 at the same Ru/pyrene ratio, here 0.029 (entry 2 in Tables 1 and 2), it is clear that the NPs have a larger quenching effect on G_1 (82%) than on G_2 (67%). This suggests that some pyrene groups of G2 are too far from the NP surface for their emission to be efficiently quenched, which might be related to the bulkiness of this pyrene-labelled dendron and to the flexibility and length of the butyl chains. In particular, the optimal ligand exchange makes the G1 dendron the best system for energy/electron transfer from the pyrene moieties of the dendrons to the NPs. At Ru/pyrene ratio = 0.058, a quenching value of 94% is observed, while only *ca.* 50% is observed for the simple Py–Ac and Py–But ligands, which further emphasizes the interesting behaviour of the G1 fluorophore.

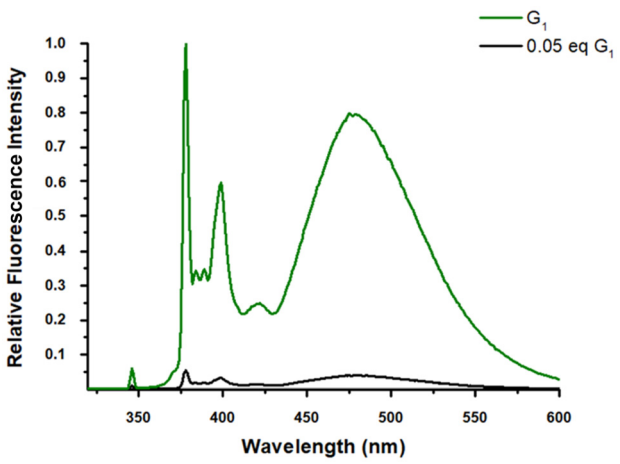

Fig. 4 Py_2–COOH (G1) emission quenching; λ_{exc} = 344 nm; slit 1.0 nm: (green) 1.8×10^{-6} M of G1; (black) 4.53×10^{-6} M of G1 – [OA–Ru NP] : [G_1] = 0.116.

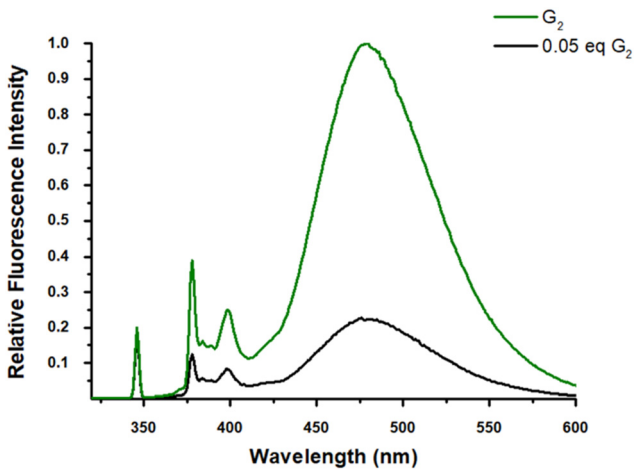

Fig. 5 Py_4–COOH (G2) fluorescence emission quenching; λ_{exc} = 344 nm; slit 1.25 nm: (green) 2.7×10^{-7} M of G2; (black) 4.40×10^{-6} M of G2 – [OA–Ru NP] : [G_2] = 0.116.

Table 1 Quenching efficiency obtained according to different [OA–Ru NP] : [G_1] ratios

G_1 added (eq.)	Relation [OA–Ru NP] : [G_1]	Relation [OA–Ru NP] : [Py unit]	Quenching efficiency (%)	G_1 in interaction (eq.)
0.15	0.038	0.019	75	0.07
0.10	0.058	0.029	82	n.d.
0.05	0.116	0.058	94	0.03

Table 2 Quenching efficiency obtained according to different [OA–Ru NP] : [G_2] ratios

G_2 added (eq.)	Relation [OA–Ru NP] : [G_2]	Relation [OA–Ru NP] : [Py unit]	Quenching efficiency (%)
0.15	0.038	0.010	61
0.05	0.116	0.029	67

3. Conclusion

This study reports the anchoring of pyrene-type fluorophores bearing carboxylic acid groups, including Fréchet-type dendrons of first and second generations, by ligand exchange at the surface of octanoic acid-stabilized Ru NPs. 2D DOSY ^{1}H NMR studies allowed us to follow the ligand exchange and study the ability of each fluorophore to interact with the NP surface. As the anchoring of the different fluorophores has been carried out on the same pre-formed NPs, it allowed a direct comparison of the optical properties of the obtained hybrid nanostructures depending on the structure of the fluorophores. After studying the anchoring of pyrene acetic acid and pyrene butyric acid as model systems, first- and second-generation Fréchet-type dendrons (G_1, Py_2–COOH) and (G_2, Py_4–COOH), containing 2 and 4 pyrene units, respectively, were successfully anchored at the surface of the NPs. The obtained dendron-functionalized NPs exhibited a significant-to-efficient quenching of the pyrene fluorescence (67% with G_2 and 94% with G_1 with respect to the free dendrons). Interestingly, the quite large distance between the photoactive centres and the metal surface was not detrimental to the fluorescence quenching phenomenon. The use of rigid, pyrene-containing Fréchet-type dendrons allows the incorporation of more pyrene units at longer distances to NPs. The question of whether the fluorescence quenching arises only from resonance energy transfer or also from electron transfer remains to be solved in order to optimize the design of these hybrid systems.

4. Experimental section

4.1. Characterization techniques

4.1.1. Nuclear magnetic resonance (NMR). Solution ^{1}H NMR experiments were performed on a Bruker Avance 300 spectrometer operating at 300 MHz and a Bruker Avance 500 spectrometer operating at 500 MHz. $CDCl_3$ was used for the characterization of the dendrons, and benzene-d_6 or THF-d_8 for the 1D and 2D DOSY ^{1}H NMR experiments related to the study of the ligand exchange. The preparation of the NMR tubes was performed by dispersing the powder of nanoparticles in the deuterated solvent under an argon atmosphere to avoid any oxidation. The spectra were internally referenced according to the solvent residual peak (δ^1H = 7.24 ppm in $CDCl_3$, and 1.76 and 3.61 ppm in THF-d_8).

On the basis of pulsed field gradient (PFG) NMR, the diffusion rate of a species in a solvent was measured by acquiring a series of spectra at incrementally increasing gradient strengths, resulting in signal attenuation caused by the self-diffusion of the molecules that was used to calculate the diffusion coefficient (D). To obtain the spectra without signals of the free ligands, a single ^{1}H NMR spectrum was measured by choosing the gradient length, gradient level, and the diffusion delay in a way that the free, sharp ligand signals would be completely attenuated, and those of the coordinated one would still be visible due to slower diffusion. For quantification of the exchange process from the diffusion coefficient-filtered DOSY spectra, the grease content at δ^1H about 0 ppm in THF-d_8 (which remained constant upon successive addition of fluorophore aliquots to the OA–Ru NPs solution) was used as an internal standard. The first spectrum, recorded in the absence of the fluorophore, was used to determine the calibration factor, C, between the integration value of grease and the number of equivalents of OA present in solution (*i.e.* 0.2 eq., as all OA introduced for the synthesis of the OA–Ru NPs remains in the powder at the end of the synthesis). After each addition of the fluorophore aliquot to the NMR tube, the NMR spectrum was analysed using the same calibration factor C. The number of coordinated fluorophores was then calculated from the integration of the aromatic signals divided by the number of hydrogen atoms on the pyrene and phenyl rings (Py: 10H, Py–Ac, Py–But: 9H, Py_2–COOH: 21H, Py_4–COOH: 45H). This allowed determination of the contribution of the fluorophore to the alkyl region of the spectra (Py–Ac: 2H, Py–But: 6H, Py_2–COOH: 16H, Py_4–COOH: 32H times the corresponding number of moles). The equivalent number of the coordinated OA molecules was then calculated from the integration of the alkyl protons, minus the contribution of the CH_2 protons from the substituted Py–L, divided by 17 (the number of protons per OA molecule). All equivalents are given *vs.* Ru content.

4.1.2. Optical properties by UV-vis and fluorescence spectroscopy. Electronic absorption spectra (UV-vis) were recorded on a Lambda 35 Perkin Elmer spectrometer within the wavelength range of 200–400 nm. Steady-state fluorescence emission spectra were registered on a FluoroMax-4 Horiba Jobin Yvon spectrofluorometer, exciting at the higher wavelength observed in the absorption spectra and scanning in the range of 300–800 nm. Excitation and emission spectra were set with a 1.25, 1.0 or 0.5 nm bandpass. Fluorescence measurements were performed on solutions with an absorbance below 0.1 to avoid self-absorbance effects. For free fluorophores, sample preparation was performed by dissolving the fluorophores in dry, degassed THF under an inert atmosphere in a glove box. The solutions were then transferred into air-tight, high-precision fluorescence cells (10 × 10 mm, Hellma Analytics) for optical measurements. Analyses were performed instantly after preparing the sample solutions. For the hybrid systems, the measurements were performed on solutions prepared as described in section 4.3.3, where the hybrid nanostructures are formed *in situ*. A screening of the fluorophore concentration in the range [Py–L] : [Ru] from 0.05 to 0.2 was applied for the preparation of the samples, such that the absorbance

was lower than 0.1 at the excitation wavelength. Relative fluorescence emission spectra are reported. The concentration of the quencher (OA–Ru NPs) was calculated by dividing the Ru molar concentration by the mean number of Ru atoms per NP, assuming their size did not change during the process (average size of 1.7 ± 0.6 nm; *ca.* 173 Ru atoms per NP). For each series, they were obtained by normalization of the emission spectra presenting the highest emission and subsequent division of all other spectra by the emission value taken at λ_{max}. Optical measurement values are reported with an error of about 10%.

4.1.3. Transmission electron microscopy (TEM). TEM analysis was performed at the "Centre de microcaractérisation Raimond Castaing" in Toulouse (UAR-CNRS 3623). TEM grids were prepared by drop-casting the crude colloidal suspension in pentane onto a holey, carbon-coated copper grid. TEM images were obtained using a JEOL 1100 electron microscope operating at 100 kV with a point resolution of 4.5 Å or a JEOL JEM 1400 operating at 120 kV. Statistical size distribution was built by analysing TEM images with ImageJ software, measuring mean diameters of >200 non-touching particles and assuming a spherical shape, and then fitting with a Gaussian function. Size distribution is quoted as the mean diameter ± twice the standard deviation (σ), which corresponds to a 95% confidence level.

4.2. Synthesis of fluorescent dendrons

4.2.1. General method and materials. Pyrene (Py; 98.0%) and pyrene acetic acid (Py–Ac; 97.0%) were purchased from Aldrich, and pyrene butyric acid (Py–But; 97.0%) from Alfa Aesar. They were dried under vacuum and stored in a glove box (MBraun) under argon (Air Liquide classe 2, U 1006) prior to use. 1-(4-Bromobutyl)pyrene **1** and dendritic benzyl bromide with two pyrene units at the periphery **3** were prepared according to previously reported procedures.[8] All reagents employed for the synthesis of Py_2–COOH and Py_4–COOH (methyl 3,5-dihydroxybenzoate, K_2CO_3, KOH, 18-crown-6) were purchased from Aldrich and used as received. Acetone was dried over $MgSO_4$.

4.2.2. Synthesis of compound 2. To a solution of 1-(4-bromobutyl)pyrene **1** (500 mg, 1.48 mmol) in anhydrous acetone (30 mL), methyl 3,5-dihydroxybenzoate (113 mg, 0.67 mmol), K_2CO_3 (464 mg, 3.36 mmol) and 18-crown-6 (catalytic amount) were added. The reaction mixture was stirred under reflux for 72 h. After this time, it was filtered over Celite and the solvent was evaporated under reduced pressure. The crude product was dissolved in dichloromethane, and the solution was washed with water. The organic phase was dried with $MgSO_4$, filtered and concentrated under reduced pressure. The crude product was purified by silica gel column chromatography with a polarity gradient (CH_2Cl_2 : hexane 1 : 1; CH_2Cl_2; CH_2Cl_2 : MeOH 99 : 1). The final product **2** was obtained as a white solid (338 mg, 74%). ^{1}H NMR (δ ppm, 400 MHz, $CDCl_3$): 8.28 (d, 2H, J = 9.2, Ar_{py}), 8.16–7.97 (m, 14H, Ar_{py}), 7.88 (d, 2H, J = 7.9, Ar_{py}), 7.17 (d, 2H, J = 2.4, H_o), 6.62 (t, 1H, J = 2.4, H_p), 4.02 (t, 4H, J = 6.1, OCH_2), 3.89 (s, 3H, CH_3), 3.41 (t, 4H, J = 7.4, Ar–CH_2), 2.09–1.92 (m, 8H, CH_2–CH_2).

4.2.3. Synthesis of Py_2–COOH. The ester of the first-generation **2** (120 mg, 0.176 mmol) was dissolved in a 3/1 ratio of THF/ethanol (24 mL), and KOH (99 mg, 1.76 mmol) was added. The reaction mixture was stirred for 2 h at reflux. The reaction mixture was cooled to room temperature, and the solvent was evaporated. The crude product was dissolved in CH_2Cl_2, and the organic phase was washed twice with HCl (2 N) and once with water, then dried over $MgSO_4$ and evaporated. Product **Py_2–COOH** was purified by crystallization in methanol and was obtained as a white solid (96 mg, 82%). ^{1}H NMR (δ ppm, 300 MHz, $CDCl_3$): 8.28 (d, 2H, J = 9.4, Ar_{py}), 8.16–7.93 (m, 14H, Ar_{py}), 7.88 (d, 2H, J = 8.8, Ar_{py}), 7.20 (d, 2H, J = 2.4, H_o), 6.65 (t, 1H, J = 2.4, H_p), 4.03 (t, 4H, J = 6.0, OCH_2), 3.42 (t, 4H, J = 7.2, Ar–CH_2), 2.09–1.94 (m, 8H, CH_2–CH_2).

4.2.4. Synthesis of compound 4. To a solution of **3** (100 mg, 0.14 mmol) in DMF (3 mL), methyl 3,5-dihydroxybenzoate (11 mg, 0.06 mmol), K_2CO_3 (194 mg, 1.40 mmol) and 18-crown-6 (catalytic amount) were added. The reaction mixture was stirred under reflux for 72 h. After this time, the solvent was evaporated under reduced pressure. The crude product was dissolved in dichloromethane, and the solution was washed with water. The organic phase was dried with $MgSO_4$, filtered and concentrated under reduced pressure. The crude product was purified by silica gel column chromatography with a polarity gradient (CH_2Cl_2 : hexane 1 : 1; CH_2Cl_2; CH_2Cl_2 : MeOH 99 : 1). The final product **4** was obtained as a white solid (59 mg, 65%). ^{1}H NMR (δ ppm, 400 MHz, $CDCl_3$): 8.24 (d, 4H, J = 9.2, Ar_{py}), 8.13–7.91 (m, 28H, Ar_{py}), 7.84 (d, 4H, J = 7.9, Ar_{py}), 7.27 (d, 2H, J = 2.1, H_o), 6.76 (t, 1H, J = 2.1, H_p), 6.51 (d, 4H, J = 2.1, H_o), 6.36 (t, 2H, J = 2.1, H_p), 4.92 (s, 4H, OCH_2–Ar), 3.94 (t, 8H, J = 6.1, OCH_2), 3.84 (s, 3H, CH_3), 3.36 (t, 8H, J = 7.4, Ar–CH_2), 2.03–1.87 (m, 16H, CH_2–CH_2).

4.2.5. Synthesis of Py_4–COOH. The ester of the second-generation **4** (50 mg, 0.03 mmol) was dissolved in a 3/1 ratio of THF/ethanol (10 mL), and KOH (20 mg, 0.35 mmol) was added. The reaction mixture was stirred for 2 h at reflux. The reaction mixture was cooled to room temperature, and the solvent was evaporated. The crude product was dissolved in CH_2Cl_2, and the organic phase was washed twice with HCl (2 M) and once with water, then dried over $MgSO_4$ and evaporated. Product **Py_2–COOH** was purified by crystallization in methanol and obtained as a white solid (17 mg, 35%). ^{1}H NMR (δ ppm, 400 MHz, $CDCl_3$): 8.23 (d, 4H, J = 9.2, Ar_{py}), 8.11–7.96 (m, 28H, Ar_{py}), 7.82 (d, 4H, J = 7.9, Ar_{py}), 7.28 (d, 2H, J = 2.2, H_o), 6.79 (t, 1H, J = 2.2, H_p), 6.50 (d, 4H, J = 2.2, H_o), 6.36 (t, 2H, J = 2.1, H_p), 4.91 (s, 4H, OCH_2–Ar), 3.94 (t, 8H, J = 6.1, OCH_2), 3.35 (t, 8H, J = 7.4, Ar–CH_2), 2.03–1.87 (m, 16H, CH_2–CH_2).

4.3. Synthesis of octanoic acid-stabilized Ru NPs (OA–Ru NPs) and hybrid systems (Py–L/OA–Ru NPs)

4.3.1. General method and materials. All operations concerning the synthesis or the preparation of samples for characterization were carried out using standard Schlenk tubes and

Fischer-Porter bottle techniques or in a glove box (MBraun) under an argon atmosphere (Air Liquide, class 2, U 1006). The ruthenium-1,5-cyclooctadiene-1,3,5-cyclooctatriene (Ru(COD)(COT)) complex was synthesized using a slightly modified procedure[48] from $RuCl_3{\cdot}xH_2O$ and cyclooctadiene, purchased from Janssen (39–43% Ru) and Aldrich (purity ≥ 99%), respectively. Other chemicals were purchased as follows: octanoic acid from Aldrich (purity ≥ 99%), pentane (RE 99%) and THF (RE 99%) from Carlo-Erba, $CDCl_3$, THF-d_8 and benzene-d_6 from Eurisotop (purity of 99.5% and 99.5%, respectively) and H_2 from Air Liquide (<3 ppm H_2O and <2 ppm O_2). Pentane and THF were purified by column filtration using MBraun purification equipment, degassed by three freeze–pump–thaw cycles and handled under an argon atmosphere. THF-d_8 and benzene-d_6 were dried over activated molecular sieves (4 Å) and stored in the glove box before use. Octanoic acid was used without purification but dried over activated molecular sieves (4 Å) before storage in a glove box.

4.3.2. Octanoic acid-stabilized Ru NPs (OA–Ru NPs). The Ru(COD)(COT) complex (30.0 mg; 0.095 mmol) was dissolved under argon in 20 mL of *n*-pentane inside a Fischer-Porter reactor, leading to a yellow solution. 0.20 molar equivalent of dry octanoic acid (2.74 mg; 0.019 mmol) was added to the reaction mixture. Then, the reactor was pressurized with 3 bar of hydrogen (H_2), and the reaction mixture was maintained at room temperature with vigorous magnetic stirring for 30 min. This led to the formation of a black colloidal suspension. After depressurization of the reactor, pentane and released cyclooctane were removed under vacuum. Redispersion/evaporation cycles in THF and then pentane were applied to obtain a dry black powder. Since OA is non-volatile, the 0.20 molar equivalents introduced initially remained in the final product. The ^{1}H NMR study (in THF-d_8) evidenced that all OA was coordinated to the NPs.

4.3.3. Hybrid systems (Py–L/OA–Ru NPs). Five different fluorophore molecules (pyrene (Py), pyrene acetic acid (Py–CH_2COOH; Py–Ac), pyrene butyric acid (Py–C_3H_6COOH; Py–But), 3,5-bis(4-pyren-1-yl-butyloxy)-benzoic acid (Py_2–COOH; G_1), and second-generation dendron (Py_4–COOH; G_2)) were coupled with the pre-formed ruthenium nanoparticles stabilized by octanoic acid. In a general procedure, a batch of pre-formed OA–Ru NPs (synthesized from 30 mg of the Ru(COD)(COT) precursor) was dissolved in dry THF-d_8 inside an NMR tube at room temperature and under an argon atmosphere. Then, a given quantity of the chosen fluorophore was added to the NMR tube, and the reaction medium was sonicated for 20 min in order to initiate the ligand exchange. A screening of the fluorophore concentration in the range [Py–L] : [Ru] from 0.05 to 0.3 was applied to optimize the ligand exchange for each case studied. This exchange was monitored by proton and DOSY ^{1}H NMR.

Author contributions

R. G. G.: synthesis of the dendrons and nanoparticle systems, analysis of the nanoparticles by TEM, ^{1}H NMR, UV-vis and fluorescence experiments, and first draft of the manuscript; M. V.: synthesis of the dendrons, analysis of the fluorescence data, compiling the corresponding figures and tables, and manuscript drafting; C. B.: recording, analysis and figure compiling from DOSY NMR; C. A.: conceptualization, resources, writing – review and editing, and supervision, E. R.: conceptualization, resources, writing – review and editing, and supervision; K. P. conceptualization, resources, writing – review and editing, supervision, and funding acquisition.

Data availability

The main data of our work are presented in the manuscript or the ESI.† Moreover, when our work is accepted for publication, the source data will be deposited as an annex in the "HAL" Repository, in the form of a Zip archive following the Open Air and F.A.I.R. data principles.

Conflicts of interest

There are no conflicts of interest to declare.

Acknowledgements

Financial support from the Centre National de la Recherche (CNRS) and the University of Toulouse 3 – Paul Sabatier is gratefully acknowledged. R. González-Gómez thanks the Associated International Laboratory (LIA) France-Mexico "LCMMC" (CNRS-CONACyT) for the internship grant. ER is grateful to PAPIIT-DGAPA (Project IN105725) and CONACyT (Project 279380) for financial support. We thank the "Centre de microcaractérisation Raimond Castaing – UAR 3623" for access to the TEM microscopes.

References

1 *Nanoparticles: From Theory to Application*, ed. G. Schmid, Wiley-VCH, Weinheim, 2nd edn, 2012.
2 B. Dubertret, M. Calame and A. J. Libchaber, Single-mismatch detection using gold-quenched fluorescent oligonucleotides, *Nat. Biotechnol.*, 2001, **19**, 365–370.
3 G. Panthi and M. Park, Synthesis of metal nanoclusters and their application in Hg2+ ions detection: A review, *J. Hazard. Mater.*, 2021, **424**, 127565.
4 Y. Li, Q. Liang, L. Zhou, *et al.*, Metal nanoparticles: a platform integrating diagnosis and therapy for rheumatoid arthritis, *J. Nanopart. Res.*, 2022, **24**, 84.
5 *Semiconductor Nanocrystals and Metal Nanoparticles Physical Properties and Device Applications*, ed. T. Chen and Y. Liu, CRD Press, Advances in Materials and Engineering, 1st edn, 2017.
6 *Metal Nanostructures for Photonics*, ed. L. Reyes Pires Kassab and C. Bartolomeu de Araujo, Elsevier Ltd., 2019.

7 Q. Wang and K. Domen, *Chem. Rev.*, 2020, **120**(2), 919–985.
8 Y. Yamada, T. Miyahigashi, H. Kotani, K. Okubo and S. Fukuzumi, *J. Am. Chem. Soc.*, 2011, **133**, 16136–16145.
9 C. Kong, Z. Li and G. Lu, *Int. J. Hydrogen Energy*, 2015, **40**, 5824–5830.
10 N. Romero, R. Guerra, L. Gil, S. Drouet, I. Salmeron, O. Illa, K. Philippot, M. Natali, J. García-Antón and X. Sala, *Sustainable Energy Fuels*, 2020, **4**, 4170–4178.
11 J. Duhamel, *Acc. Chem. Res.*, 2006, **39**, 953–960.
12 J. Duhamel, *Polymers*, 2012, **4**, 211–239.
13 J. Duhamel, *Langmuir*, 2012, **28**, 6527–6538.
14 F. Winnik, *Chem. Rev.*, 1993, **93**, 587–614.
15 R. S. Sprick, J. X. Jiang, B. Bonill, S. Ren, T. Ratvijitvech, P. Guiglion, M. A. Zwijnenburg, D. J. Dams and A. L. J. Cooper, *J. Am. Chem. Soc.*, 2015, **137**, 3265.
16 W. Chen, N. B. Zuckerman, J. W. Lewis, J. P. Konopelski and S. Chen, *J. Phys. Chem. C*, 2009, **113**, 16988–16995.
17 W. Chen, N. B. Zuckerman, J. P. Konopelski and S. Chen, *Anal. Chem.*, 2010, **82**, 461–465.
18 X. Kang, W. Chen, N. B. Zuckerman, J. P. Konopelski and S. Chen, *Langmuir*, 2011, **27**, 12636–12641.
19 P. Hu, L. Chen, X. Kang and S. Chen, *Acc. Chem. Res.*, 2016, **49**, 2251–2260.
20 E. Morais, C. Moloney, C. O'Modhrain, E. McKiernan, D. F. Brougham and J. A. Sullivan, *Chem. – Eur. J.*, 2021, **27**, 1023–1030.
21 S. R. Barman, A. Nain, S. Jain, N. Punjabi, S. Mukherji and J. Satija, *J. Mater. Chem. B*, 2018, **6**, 2368–2384.
22 S. Deng, T. M. Fulghum, G. Krueger, D. Patton, J. Park and R. C. Advincula, *Chem. – Eur. J.*, 2011, **17**, 8929–8940.
23 A. Harriman, *Chem. Commun.*, 2015, **51**, 11745–11756.
24 D. Astruc, E. Boisselier and C. Ornelas, *Chem. Rev.*, 2010, **110**, 1857–1959.
25 G. Zaragoza-Galán, M. A. Fowler, J. Duhamel, R. Rein, N. Solladié and E. Rivera, *Langmuir*, 2012, **28**, 11195–11205.
26 G. Zaragoza-Galán, M. Fowler, R. Rein, N. Solladié, J. Duhamel and E. Rivera, *J. Phys. Chem. C*, 2014, **118**, 8280–8294.
27 G. Zaragoza-Galán, J. Ortíz-Palacios, B. X. Valderrama, A. A. Camacho-Dávila, D. Chávez-Flores, V. H. Ramos-Sánchez and E. Rivera, *Molecules*, 2014, **19**, 352–366.
28 S. M. Rojas-Montoya, M. Vonlanthen, P. Porcu, G. Flores-Rojas, A. Ruiu, D. Morales-Morales and E. Rivera, *Dalton Trans.*, 2019, **48**, 10435–10447.
29 P. Porcu, M. Vonlanthen, I. González-Méndez, A. Ruiu and E. Rivera, *Molecules*, 2018, **23**(9), 2289.
30 A. García-Rodríguez, P. Porcu, A. S. Estrada-Montaño, M. Vonlanthen, R. D. Martínez-Serrano, G. Zaragoza-Galán and E. Rivera, *Dyes Pigm.*, 2021, **185**, 108925.
31 Y. Bañales-Leal, A. García-Rodríguez, F. Cuétara-Guadarrama, M. Vonlanthen, K. Sorroza-Martínez, D. Morales-Morales and E. Rivera, *Dyes Pigm.*, 2021, **191**, 109382.
32 T. M. Figueira-Duarte and K. Müllen, *Chem. Rev.*, 2011, **111**, 7260–7314.
33 P. Lara, K. Philippot and B. Chaudret, *ChemCatChem*, 2013, **5**, 28–45.
34 M. R. Axet and K. Philippot, *Chem. Rev.*, 2020, **120**(2), 1085–1145.
35 C. Amiens, B. Chaudret, D. Ciuculescu-Pradines, V. Collière, K. Fajerwerg, P. Fau, M. Kahn, A. Maisonnat and K. Philippot, *New J. Chem.*, 2013, **37**(11), 3374–3401.
36 C. Amiens, D. Ciuculescu-Pradines and K. Philippot, *Coord. Chem. Rev.*, 2016, **38**, 409–432.
37 P.-J. Debouttière, V. Martinez, K. Philippot and B. Chaudret, *Dalton Trans.*, 2009, 10172–10174.
38 R. Estivill, D. Ciuculescu, C. Amiens, M. Comesaña-Hermo, M. Farle, P. Batat, G. Jonusauskas, N. D. McClenaghan, P. Lecante, C. Tardin and S. Mazeres, *ChemPhysChem*, 2011, **12**, 2915–2919.
39 W. Chen, N. B. Zuckerman, J. W. Lewis, J. P. Konopelski and S. Chen, *J. Phys. Chem. C*, 2009, **113**, 16988–16995.
40 J. De Tovar, N. Romero, S. Denisov, R. Bofill, C. Gimbert-Suriñach, D. Ciuculescu-Pradines, S. Drouet, A. Llobet, P. Lecante, V. Colliere, Z. Freixa, N. McClenaghan, C. Amiens, J. García-Antón, K. Philippot and X. Sala, *Mater. Today Energy*, 2018, **9**, 506–515.
41 Q. T. Nguyen, E. Rousset, V. T. H. Nguyen, V. Colliere, P. Lecante, W. Klysubun, K. Philippot, J. Esvan, M. Respaud, G. Lemercier, P. D. Tran and C. Amiens, *ACS Appl. Mater. Interfaces*, 2021, **13**(45), 53829–53840.
42 A. Oliva-Puigdomènech, J. De Roo, J. Kuhs, C. Detavernier, J. C. Martins and Z. Hens, *Chem. Mater.*, 2019, **31**, 2058–2067.
43 M. R. Axet and K. Philippot, *Chem. Rev.*, 2020, **120**(2), 1085–1145.
44 R. González-Gómez, L. Cusinato, C. Bijani, Y. Coppel, P. Lecante, C. Amiens, I. del Rosal, K. Philippot and R. Poteau, *Nanoscale*, 2019, (11), 9392–9409.
45 R. González Gómez, PhD of Université de Toulouse 3 – Paul Sabatier, 2019.
46 P. P. H. Cheng, D. Silvester, G. Wang, G. Kalyuzhny, A. Douglas and R. W. Murray, *J. Phys. Chem. B*, 2006, **110**, 4637–4644.
47 E. Dulkeith, A. C. Morteani, T. Niedereichholz, T. A. Klar, J. Feldmann, S. A. Levi, F. C. J. M. van Veggel, D. N. Reinhoudt, M. Möller and D. I. Gittins, *Phys. Rev. Lett.*, 2002, **89**, 203002.
48 P. Pertuci and G. Vitulli, *Inorg. Synth.*, 1983, **22**, 178.